



# Crystal Structure of Arrestin-3 Reveals the Basis of the Difference in Receptor Binding Between Two Non-visual Subtypes

Xuanzhi Zhan<sup>1</sup>, Luis E. Gimenez<sup>1</sup>, Vsevolod V. Gurevich<sup>1\*</sup>  
and Benjamin W. Spiller<sup>1,2\*</sup>

<sup>1</sup>Department of Pharmacology, Vanderbilt University, Nashville, TN 37232, USA

<sup>2</sup>Department of Microbiology and Immunology, Vanderbilt University, Nashville, TN 37232, USA

Received 3 October 2010;

received in revised form

2 December 2010;

accepted 21 December 2010

Available online

6 January 2011

Edited by I. Wilson

## Keywords:

arrestin;

stability;

BRET;

self-association;

GPCR

Arrestins are multi-functional proteins that regulate signaling and trafficking of the majority of G protein-coupled receptors (GPCRs), as well as sub-cellular localization and activity of many other signaling proteins. We report the first crystal structure of arrestin-3, solved at 3.0 Å resolution. Arrestin-3 is an elongated two-domain molecule with overall fold and key inter-domain interactions that hold the free protein in the basal conformation similar to the other subtypes. Arrestin-3 is the least selective member of the family, binding a wide variety of GPCRs with high affinity and demonstrating lower preference for active phosphorylated forms of the receptors. In contrast to the other three arrestins, part of the receptor-binding surface in the arrestin-3 C-domain does not form a contiguous  $\beta$ -sheet, which is consistent with increased flexibility. By swapping the corresponding elements between arrestin-2 and arrestin-3 we show that the presence of this loose structure is correlated with reduced arrestin selectivity for activated receptors, consistent with a conformational change in this  $\beta$ -sheet upon receptor binding.

© 2011 Elsevier Ltd. All rights reserved.

## Introduction

Mammals express four arrestin proteins<sup>†,1</sup>. In contrast to highly specialized visual arrestin-1 and arrestin-4, which are selectively expressed at very

high levels in photoreceptors and bind rhodopsin and cone opsins,<sup>2–4</sup> the two non-visual subtypes are present in virtually every cell, and interact with hundreds of G protein-coupled receptors (GPCRs).<sup>5</sup> In most cases, arrestin-2 outnumbers arrestin-3 by 10~20:1.<sup>6,7</sup> Non-visual arrestins also serve as multi-functional adaptors, linking GPCRs to the endocytic machinery<sup>8,9</sup> and directing signaling to mitogen-activated protein kinases and Src family kinases, as well as orchestrating protein ubiquitination (for reviews see Refs. 5 and 10). Direct studies of the binding of different arrestins to the four functional states of their cognate receptors (active phosphorylated, inactive phosphorylated, active unphosphorylated and inactive unphosphorylated) revealed striking differences in their selectivity. Arrestin-1 has a remarkable preference for active phosphorylated receptor over inactive phosphoreceptor with >10-fold difference in binding,<sup>11,12</sup>

\*Corresponding authors. E-mail addresses:  
[vsevolod.gurevich@vanderbilt.edu](mailto:vsevolod.gurevich@vanderbilt.edu);

[benjamin.spiller@vanderbilt.edu](mailto:benjamin.spiller@vanderbilt.edu).

<sup>†</sup> We use systematic names of arrestin proteins: arrestin-1 (historically called S-antigen, 48kDa protein, and visual or rod arrestin), arrestin-2 ( $\beta$ -arrestin or  $\beta$ -arrestin1), arrestin-3 ( $\beta$ -arrestin2), and arrestin-4 (cone or X-arrestin).

Abbreviations used: GPCR, G protein-coupled receptor; GRP-R, gastrin-releasing peptide receptor; IP6, inositol 6-phosphate; BRET, bioluminescence resonance energy transfer.

while non-visual arrestins show <2-fold difference in binding levels at best.<sup>13–15</sup> Non-visual arrestins also show a much smaller preference for phosphorylated over unphosphorylated active receptors than arrestin-1.<sup>13,16</sup> In both regards, arrestin-3 is the least selective.

Single non-visual arrestin knockout mice are grossly normal, whereas the double arrestin-2/3 knockout is embryonic lethal,<sup>17</sup> suggesting that these subtypes are redundant to some extent. However, arrestin-3 demonstrates higher affinity for many GPCRs,<sup>17,18</sup> as well as clathrin,<sup>8</sup> and has a number of unique functions.<sup>5,10</sup> Crystal structures of arrestin-1,<sup>19,20</sup> arrestin-2<sup>21–24</sup> and arrestin-4<sup>25</sup> have been determined, making the structure of this intriguing subtype the only one missing. Here, we report the first crystal structure of bovine arrestin-3, determined at 3.0 Å resolution (Table 1). While the overall fold of arrestin-3 resembles that of the other family members, we identified an element on the receptor-binding concave surface of the C-domain<sup>26</sup> that is significantly different from its closest homologue, arrestin-2. By swapping this element between non-visual arrestins, we demonstrate that this structural difference contributes significantly to the differential receptor binding of the two subtypes. The structure of arrestin-3 also allowed us to identify a highly conserved self-association interface in the arrestin family.

**Table 1.** Data collection and refinement statistics

<b>A. Data collection</b>	
Space group	<i>P</i> 2 <sub>1</sub> 2 <sub>1</sub> 2 <sub>1</sub>
Cell parameters (Å)	
<i>a</i> (Å)	73.18
<i>b</i> (Å)	73.32
<i>c</i> (Å)	201.97
α = β = γ (°)	90.00
Resolution (Å)	3.0
<i>R</i> <sub>sym</sub> (%)	4.4(83)
<i>I</i> / <i>σI</i>	24(1.8)
Completeness (%)	92.7(94.4)
Redundancy	5.2(5.2)
<b>B. Refinement</b>	
Resolution range (Å)	35–3.0
No. reflections	20,879
<i>R</i> <sub>factor</sub> (%)	22.1
<i>R</i> <sub>free</sub> (%)	28.6
No. protein atoms	5611
RMSD from ideality	
Bond lengths (Å)	0.011
Bond angles (°)	1.508
Mean coordinate error	
Luzzati plot (Å)	0.36
σ <sub>A</sub> (Å)	0.37
Maximum likelihood (Å)	0.40
Ramachandran plot	
Favored (%)	97.6
Allowed (%)	1.3
Outliers (%)	1.1

## Results

### Conservation of the “arrestin fold”

The arrestin-3 structure is largely similar to that of the other arrestins (Fig. 1a). It is composed of two seven-stranded β sandwiches, termed the N-terminal and C-terminal domains, connected by a 10-residue linker (hinge region<sup>27</sup>). The carboxy terminus folds back toward the N-terminal domain, becomes unstructured for ~35 residues and forms a highly conserved tripartite interaction with the N-terminal domain consisting of two hydrophobic interactions with β-strand I and α-helix I and one buried ion pair constituting part of the main arrestin phosphate sensor, the polar core.<sup>20,28</sup> Sequence and structural alignments of arrestin-1, -2 and -3 are shown in Fig. 1, with key functional elements highlighted. The structure of the polar core, as well as the positions of other known phosphate-binding residues are well conserved between arrestin-3 and -2, as could be expected from the functional conservation of phosphate-sensing mechanisms in the arrestin family.<sup>14,15,28</sup> The concave sides of the two arrestin domains contain elements that interact with other parts of the receptor.<sup>13,26,29–31</sup> The two key “receptor discriminator” regions (N-domain and C-domain elements) responsible for receptor preference of arrestin proteins constitute parts of this surface in the N- and the C-domain.<sup>26</sup> A key difference between arrestin-3 and arrestin-2 is that the outermost “strand” in the C-domain element, residues 250–259, although well ordered (Fig. 2a) is displaced from the position it occupies in arrestin-2. The displacements of C<sup>α</sup> atoms for V257, E258, Q259 and D260 are 1.3 Å, 2.2 Å, 2.0 Å and 2.0 Å, respectively. Although these shifts are relatively small, they are about three to five times greater than the estimated positional error of the coordinates (Table 1), and occur in a region known to be essential for receptor binding.<sup>26</sup> The shift results in the loss of two H-bonds within the C-domain element (Fig. 2b), consistent with a lower energy barrier for reorganization of this region. The distorted H-bonds are between Q259 and I232, resulting in distances of 4.9 Å between the Q259 carbonyl oxygen and the Q232 amide nitrogen and 4.2 Å between the Q259 amide nitrogen and the I232 carbonyl oxygen. The alignment of previously determined structures indicates that the N-domain element exists in multiple conformations when multiple views of identical proteins are afforded by either non-crystallographic symmetry or from multiple solved structures (Fig. 2c),<sup>19–24</sup> indicating that the N-domain element is inherently flexible and therefore structural differences in this region are unlikely to be particularly informative. In contrast, the structure of the C-domain element is highly

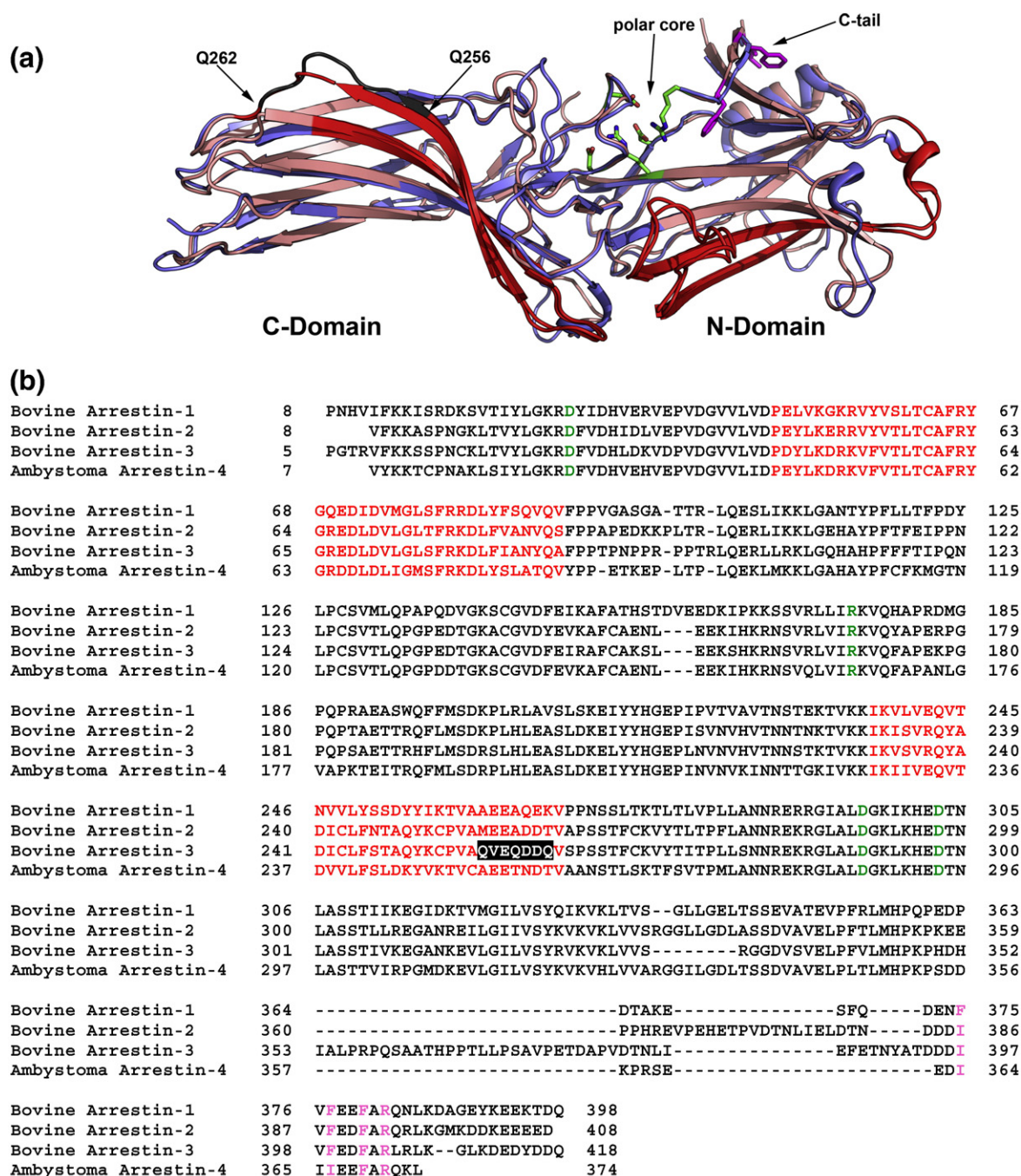
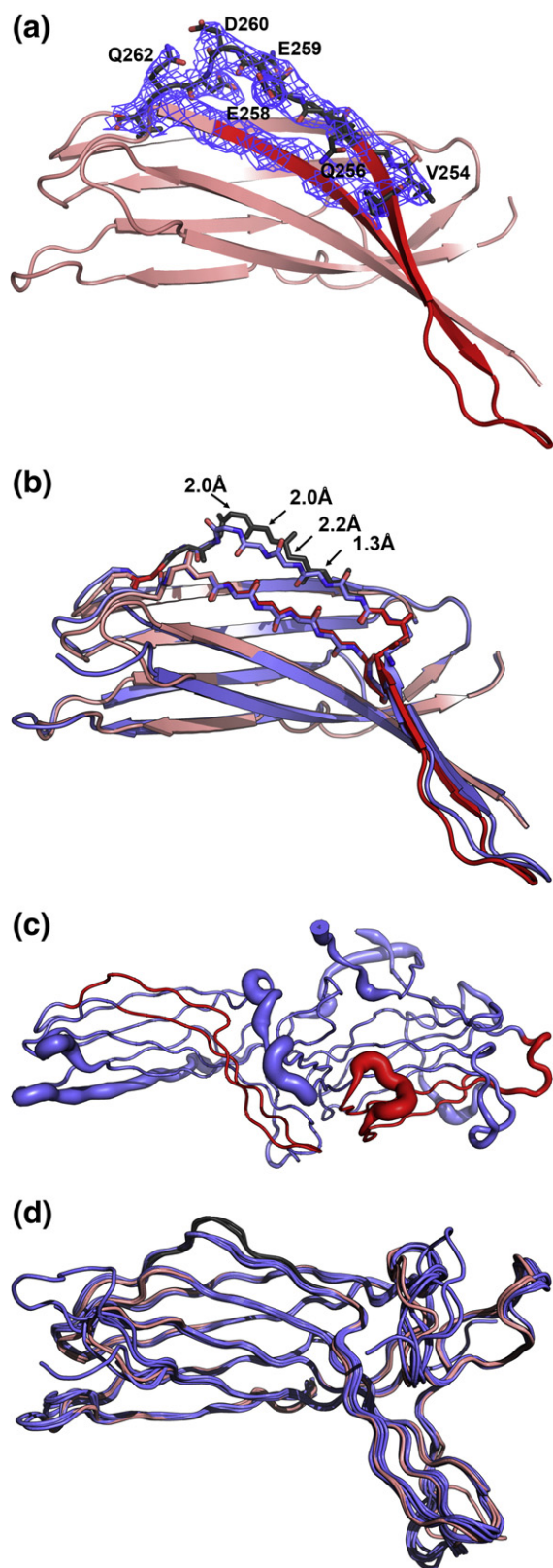


Fig. 1. Comparison of arrestin-3 to other arrestins. The N-domain element and the C-domain element, which are important for receptor specificity, are shown in red. Residues important for locking the C-terminus to the N-terminal domain and critical polar core residues are shown as (a) sticks and (b) as colored residues, with the polar core residues shown in green and the C-terminal tail residues shown in magenta. The residues in the arrestin-3 C-element that do not form a proper  $\beta$ -sheet are shown in (a) gray and (b) white on black highlight. (a) Structural overlay of arrestin-2 (blue) and arrestin-3 (salmon). (b) Sequence alignment of arrestins with solved structures.

conserved (Fig. 2c). An overlay of the C-domain from all non-visual arrestins (there are 10 crystallographically unique arrestin-2 structures: 1g4r, 1zsh, 1jsy, 3gc3 and two non-identical molecules in each

of 1g4m, 3gdi, and 2wtr),<sup>21–24</sup> shows that in all cases, arrestin-2 forms a complete  $\beta$ -sheet in the C-domain element, whereas both versions of arrestin-3 in our asymmetric unit form a distorted  $\beta$ -sheet (Fig. 2d).





### Structurally distinct receptor-binding surface contributes to decreased arrestin-3 specificity for active receptor

The arrestin-3 structure reveals that despite very similar overall architecture, the C-domain  $\beta$  sandwich is distorted, resulting in a distinct conformation of the C-domain region implicated in receptor binding (Fig. 2).<sup>26</sup> This difference occurs in a region of the structure that is otherwise well ordered, as judged by the difference in electron density (Fig. 2a). The distorted strand does not make canonical  $\beta$ -sheet hydrogen bond contacts with the rest of the C-domain element (Fig. 2b), consistent with a less stable sheet. This sets arrestin-3 apart from the other three vertebrate arrestin subtypes with known structure. Since this is the first distinguishing structural feature of the receptor-binding elements in any arrestin, we tested the functional consequences of the “relaxed” conformation of this element in arrestin-3.

Arrestins are highly homologous proteins demonstrating remarkable conservation of the positions of all known functionally important residues from *Caenorhabditis elegans* to mammals.<sup>1</sup> Due to this conservation, chimeras between different arrestin family members fold properly and retain functionality.<sup>11,13,32</sup> Therefore, we exchanged the region with distinct structure (residues 233–261 and 234–262 in arrestin-2 and -3, respectively) between the two non-visual arrestins, generating arrestin-2-6M and arrestin-3-6M mutants. Due to the high degree of homology, this is equivalent to the mutation of six residues (V234I, S246N,

**Fig. 2.** Arrestin-3 has a uniquely distorted C-domain element. The N-domain element and the C-domain element, which are important for receptor specificity, are shown in red. The residues in the arrestin-3 C-domain element that do not form proper  $\beta$ -sheet hydrogen bonding are shown in gray. (a) The distorted region of the C-domain element is well ordered and displays clear electron density. A composite omit map drawn at 1.5  $\sigma$  is shown. (b) Overlay of arrestin-2 (1g4r, blue) and arrestin-3 (salmon), showing the deviation from standard  $\beta$ -sheet geometry. Distances between C $\alpha$  positions in arrestin-2 and arrestin-3 are shown (c) A sausage representation of a calculated average arrestin-2 structure, based on the 10 crystallographically independent arrestin-2 structures. The sausage thickness corresponds to the average deviation of the eight structures from the average structure calculated with THESEUS.<sup>80</sup> Receptor discriminator elements are shown in red, with the C-domain element on the left and the N-domain element on the right, showing that although the N-domain element is variable, the C-domain element in arrestin-2 is structurally conserved. (d) Alignment of 10 distinct arrestin-2 structures (blue, from 1g4r, 1g4m, 1zsh, 1jsy, 3gdi, 3gc3 and 2wtr) with the two arrestin-3 structures present in the asymmetric unit (salmon), indicating that all other arrestins form a contiguous  $\beta$ -sheet in the C-terminal domain.

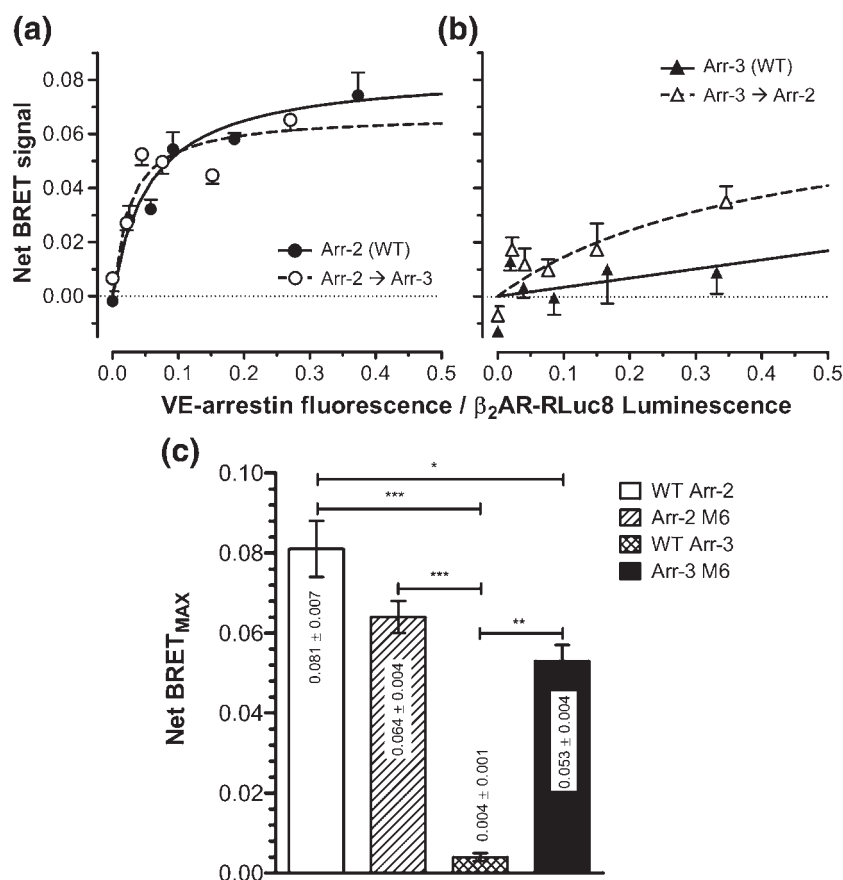


**Fig. 3.** Exchange of the structurally different C-domain receptor-binding element between arrestin-2 and arrestin-3 changes their binding to  $\beta_2$ AR in intact cells. (a) BRET signal as a function of wild type Venus-arrestin-2 (filled circles, continuous line) and the Venus-arrestin-2-6M mutant (I233V, N245S, M255Q, E256V, A258Q and T261Q; open circles, broken line) co-expression with  $\beta_2$ AR-RLuc in COS-7 cells. (b) BRET signal as a function of wild type Venus-arrestin-3 (filled triangles, continuous line) and the Venus-arrestin-3-6M mutant (V234I, S246N, Q256M, V257E, Q259A and Q262A; open circles, broken line) co-expression with  $\beta_2$ AR-RLuc in COS-7 cells. Shown is the difference between the BRET signal in the presence and in the absence of the 25  $\mu$ M  $\beta_2$ AR agonist isoproterenol, which reflects agonist-induced increase in Venus-arrestin interaction with a fixed amount of  $\beta_2$ AR-RLuc. Mean  $\pm$  S.E. of one representative experiment (out of three) done in quadruplicate are shown in (a) and (b). (c) The average BRET<sub>MAX</sub> as estimated from the fits of a one-site binding

hyperbola to the data of the binding of the indicated arrestins to the  $\beta_2$ AR. Mean  $\pm$  S.E. of three independent experiments are shown. The differences between the BRET<sub>MAX</sub> values were assessed by one-way ANOVA, followed by the Bonferroni *post hoc* test. Significance of the differences is indicated as follows: \* $p$ <0.05, \*\* $p$ <0.01, \*\*\* $p$ <0.001.

Q256M, V257E, Q259A and Q262T in arrestin-3; I233V, N245S, M255Q, E256V, A258Q and T261Q in arrestin-2). Receptor binding of these chimeras was compared to parental wild type proteins in intact cells using arrestins tagged with Venus (enhanced YFP<sup>33</sup>) on the N-terminus and  $\beta_2$ -adrenergic receptor ( $\beta_2$ AR) C-terminally tagged with Renilla luciferase in COS-7 cells. We chose  $\beta_2$ AR because both non-visual arrestins interact with this receptor *in vitro*, in *Xenopus* oocytes and in cultured cells.<sup>13–18,34</sup> One distinct functional feature of arrestin-3 is that it demonstrates a much smaller difference than arrestin-2 in binding to inactive and active GPCRs when the receptor is phosphorylated.<sup>13–15</sup> Arrestin recruitment to the receptor is reflected in bioluminescence resonance energy transfer (BRET) from luciferase to Venus, which saturates with increasing Venus-arrestin expression (Fig. 3).<sup>35–37</sup> This assay allows measurement of arrestin interactions with receptors with or without agonist stimulation in the physiological conditions of an intact cell. We found that in this cell-based assay, arrestin-3 shows a stronger agonist-independent binding to  $\beta_2$ AR than that of arrestin-2, and a correspondingly much

smaller agonist-induced increase in net BRET signal (Fig. 3). The introduction of six arrestin-2 residues into arrestin-3 significantly boosted the agonist-induced arrestin- $\beta_2$ AR interaction (Fig. 3b), whereas introducing the corresponding arrestin-3 residues into arrestin-2 somewhat reduced it (Fig. 3a). The data suggest that the absence of a proper  $\beta$ -strand in this region of arrestin-3 is likely to destabilize the receptor binding face of the  $\beta$ sandwich, allowing it to more readily adopt the “active” conformation, thereby reducing the requirement for receptor activation. Interestingly, charge reversal mutation K257E in a homologous region of arrestin-1 was found to greatly decrease its selectivity, dramatically increasing the binding to both non-preferred forms of its cognate receptor, phosphorylated inactive and light-activated unphosphorylated rhodopsin.<sup>31</sup>

### Intersubunit interface in arrestin-3 crystals

The oligomeric interactions of arrestins are thought to be functionally important, although the nature of the biologically relevant oligomers is unknown for most arrestins. Nevertheless, self-

association appears to be a key feature of arrestins, and has been documented for arrestin-1,<sup>38,39</sup> -2 and -3.<sup>23,40</sup> Arrestin-4 is the only family member known to be a constitutive monomer.<sup>40</sup> The analysis of all arrestin structures reveals one common, highly

conserved interface present in crystal forms of arrestins-1, -2 and -3. This interface is formed via a parallel  $\beta$ -sheet interaction between the first strand on the concave face of the N-terminal domain and the first strand on the convex face of

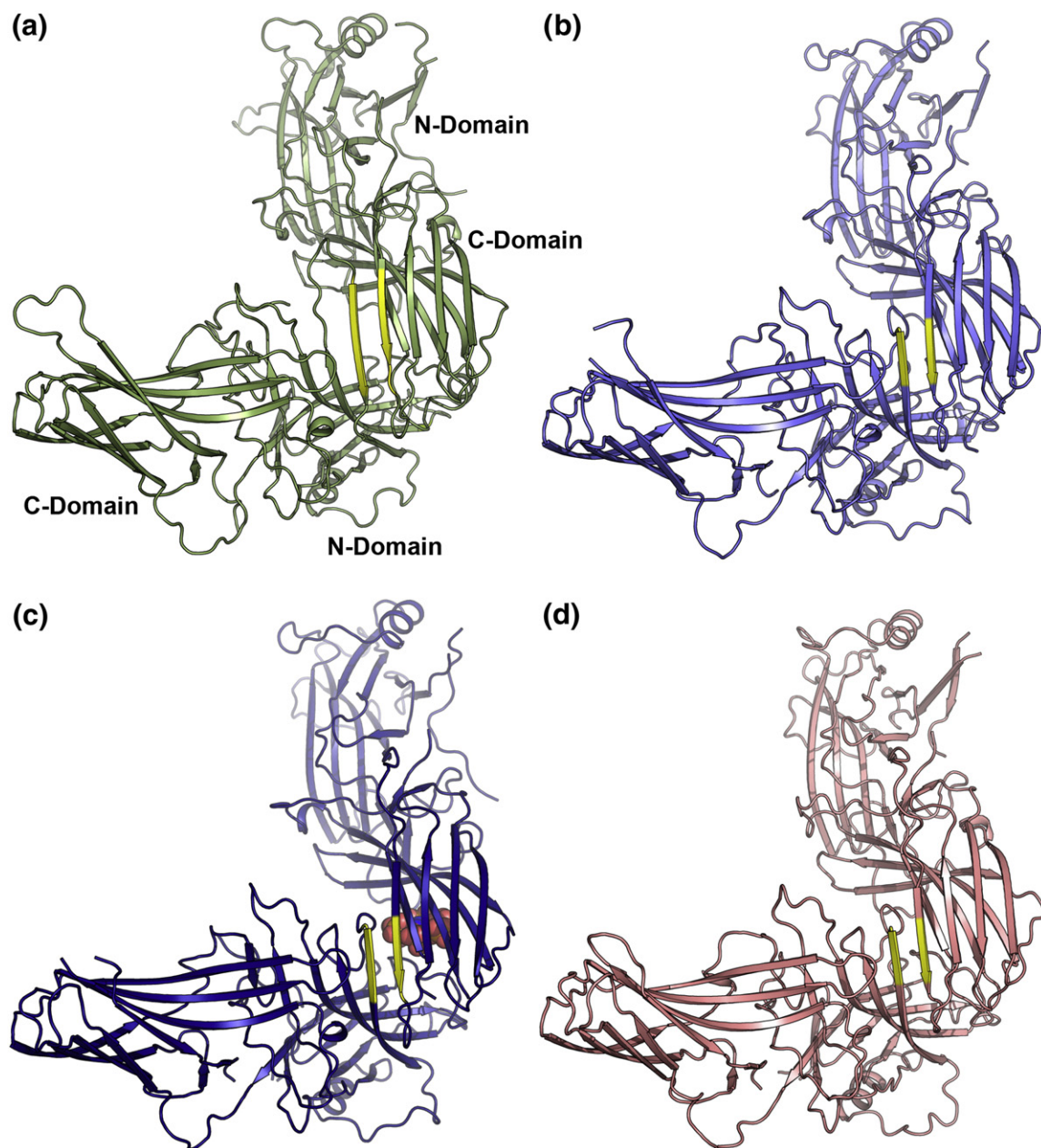


**Fig. 4.** Conserved packing interface. The interface (colored yellow) is a parallel  $\beta$ -sheet interaction between the first strand on the concave face of the N-terminal domain and the first strand on the convex face of the C-terminal domain. The length of the interaction and the residues involved vary. (a) In arrestin-1 (1cf1, green), six residues from each monomer participate, and each monomer buries  $\sim 1017 \text{ \AA}^2$ . (b) In arrestin-2 (1g4r, light blue) three residues from each monomer participate, with each arrestin-2 monomer burying  $\sim 726 \text{ \AA}^2$ . (c) In the arrestin-2-IP6 structure (1zsh, dark blue), four residues from each monomer participate, with each arrestin-2 monomer burying  $\sim 585 \text{ \AA}^2$ . IP6 is drawn as space-filling spheres and is visible in the background, behind the C-terminal  $\beta$ -sandwich, packed between N-terminal and C-terminal domains, in a binding site formed by dimerization. (d) In arrestin-3 (3P2D, salmon), three residues from each monomer participate and each monomer buries  $666 \text{ \AA}^2$ .



the C-terminal domain (Fig. 4). This interface is observed in multiple crystal forms of arrestin-1 (1cf1 and 1ary),<sup>19,20</sup> arrestin-2 (1g4r, and the related 1g4m, 1zsh and 1jsy),<sup>21,23,24</sup> the co-crystal of arrestin-2 with the clathrin NT domain (3gc3)<sup>22</sup> as well as the arrestin-3 crystals reported here. The only crystal forms in which this interface is not conserved are arrestin-4 (1suj)<sup>25</sup> and an alternative crystal of the arrestin-2-clathrin NT domain complex (3gd1).<sup>22</sup> The surface area buried by each partner in this conserved interface varies from  $\sim 1017 \text{ \AA}^2$  for arrestin-1 (1cf1) to  $\sim 494 \text{ \AA}^2$  for arrestin-2 bound to clathrin (3gc3). Frequently (85% of the time), interfaces of greater than  $\sim 850 \text{ \AA}^2$  (per partner) represent biologically relevant dimerization interfaces,<sup>41</sup> indicating that the 1cf1 interface is likely to be biologically important. We note here that this interface is frequently small,  $\sim 666 \text{ \AA}^2$  in arrestin-3, but it is conserved among all arrestins known to form oligomers and it is not conserved in the cone arrestin, which is a constitutive monomer,<sup>25,40</sup> or among the arrestin-like retromer subunit Vps26 proteins.<sup>42,43</sup> Further, inositol-6-phosphate (IP6), which is known to promote oligomerization of arrestin-2 and arrestin-3, binds between protomers in a binding pocket formed by oligomerization at this interface (Fig. 4c).<sup>22,40</sup>

## Discussion

Several lines of evidence suggest partial functional redundancy between arrestin-2 and arrestin-3; expression of the two non-visual arrestins in many tissues and cell types significantly overlap,<sup>6,7,44,45</sup> both bind many GPCRs with comparable affinity<sup>13,34</sup> and they can substitute for each other in single isoform knockout mice.<sup>17</sup> However, recent findings revealed significant functional differences; arrestin-2 promotes RhoA activation in conjunction with  $G_{\alpha_{q/11}}$ <sup>46</sup> and IGF-1-mediated activation of phosphatidylinositol-3-kinase.<sup>47</sup> A difference between the receptor-bound conformations of arrestin-2 and arrestin-3 was recently reported.<sup>48</sup> This study also noted a conserved conformational change that occurs upon activation of both arrestin-2 and arrestin-3 and involves increased protease accessibility of the region between amino acids 180 and 250 in both isoforms, consistent with increased flexibility of this region upon arrestin activation. Furthermore, different trafficking routes for agonist-activated gastrin-releasing peptide receptor (GRP-R)-arrestin-2 and GRP-R-arrestin-3 complexes were reported.<sup>49</sup> Arrestin-3 internalizes with GRP-R to endosomes, whereas arrestin-2 dissociates from the GRP-R near the plasma membrane. However, there was virtually no mechanistic or structural insight into the functional differences between arrestin-2 and arrestin-3.

The structure of bovine arrestin-3 reported here completes the structural inventory of this protein family. The overall structure is very similar to other arrestins, both in terms of the individual domains and the structural relationship between these domains (rmsd  $0.8 \text{ \AA}$  for arrestin-3 to arrestin-2 (1G4M) using 282 core  $C^\alpha$  positions). The key phosphate-sensitive interactions holding the relative orientation of the two domains, the inter-domain polar core and the three-element interaction between the C-tail,  $\beta$ -strand I and  $\alpha$ -helix I are well conserved (Fig. 2). Although inter-domain flexibility appears to be an important functional feature of arrestins,<sup>27</sup> the relative orientation of the two domains in the basal state is conserved in the family (Fig. 1a). Differences in inter-domain orientation have been reported only in the active receptor-bound state, which is expected to be quite different from the basal conformation of free arrestin.<sup>50</sup> The relaxed conformation within the C-domain receptor-binding element (Fig. 2b) of arrestin-3 sets it apart from other isoforms. Our experiments show that swapping this element between arrestin-2 and arrestin-3 shifts the preference of the resulting chimera for the active receptor towards that of the donor arrestin (Fig. 3), indicating an important role of the flexibility of this region in receptor binding. Indeed, the K257E mutation in this area in the most specific member of the family, arrestin-1, resulted in several-fold increases in binding to phosphorylated inactive and active unphosphorylated rhodopsin, thereby significantly reducing its selectivity for the activated phosphorylated form.<sup>31</sup> Interestingly, within one residue of this distorted element there are one or two amino acid insertions in the invertebrate arrestins, from *C. elegans* to *Drosophila* spp.,<sup>1</sup> some of which were shown to bind unphosphorylated receptors. Collectively, these data support the idea that the rigidity of the C-domain element is a prerequisite for high arrestin selectivity for active phosphoreceptors. Importantly, this element is part of the more compact C-domain, which invariably is more rigid, as judged by differences between atomic positions of multiple structures (Fig. 2c), than the N-domain, which contains key phosphate-binding elements involved in the activation of arrestin.<sup>28,51</sup> It is tempting to speculate that an inherently more flexible receptor-binding surface contributes to a better ability of arrestin-3 to "fit" numerous GPCRs, as reflected in its higher affinity for many receptors.<sup>17,18</sup> This structural difference is likely to affect the stability of the  $\beta$ -sandwich core of the C-domain and it might underlie known differences in the binding of non-receptor partners engaging this part of the arrestin molecule. MAP kinases c-Raf1, MEK1, ERK2, ASK1, MKK4 and JNK3<sup>52</sup> as well as ubiquitin ligase Mdm2<sup>53</sup> interact with both domains of the two non-visual arrestins. Despite similar binding,<sup>54</sup> arrestin-3, but not arrestin-2, promotes activation of JNK3,<sup>32,52,55</sup>

indicating that it arranges the three kinases in the complex differently. The distinct structure of arrestin-3 might contribute to the biologically important functional differences. Identification of the binding sites for these kinases and other non-receptor partners of arrestin proteins is necessary to test this idea.<sup>56</sup>

All arrestins, except of cone-specific arrestin-4,<sup>40</sup> oligomerize. Self-association of arrestin-1 was described (under the name of S-antigen) even before its role in the regulation of rhodopsin was established.<sup>57</sup> Arrestin-1 cooperatively forms tetramers in solution,<sup>39,58</sup> where the receptor-binding elements of all monomers are shielded by sister subunits.<sup>59</sup> Not surprisingly, only monomeric arrestin-1 binds rhodopsin,<sup>58</sup> although the oligomers retain the ability to bind microtubules,<sup>58</sup> which serve as the default arrestin-1 "parking space" in the dark-adapted rod.<sup>60,61</sup> Oligomerization of arrestin-2 has been observed in some crystal forms,<sup>21,22,24</sup> including one (1zsh)<sup>23</sup> where inositol 6-phosphate (IP6), interacting with parts of the receptor-binding surface, was found to fit perfectly between monomers in a pocket formed by a conserved interface (Fig. 4c).<sup>23</sup> Indeed, IP6 was shown to promote self-association of purified arrestin-2<sup>40</sup> and elimination of IP6-binding positive charges reduced its oligomerization within cells.<sup>23</sup> Similar observations with arrestin-3 led to the idea that its inter-subunit interface resembles that of arrestin-2.<sup>23</sup> As shown in Fig. 4, this oligomerization interface is conserved in the arrestin-3 structure described here. Although various ideas have been proposed,<sup>23,40,62</sup> the biological role of homo- and possibly hetero-oligomerization of non-visual arrestins and the ability of the oligomers to bind GPCRs remains unknown (reviewed in Ref. 63). The role of this interface in arrestin-3 oligomerization in solution needs to be tested experimentally.

## Materials and Methods

### Expression and purification of arrestin-3 and its truncation mutant

cDNA encoding bovine arrestin-3 was cloned in frame in the pTrcHisB vector (Invitrogen; Carlsbad, CA) between NcoI and HindIII sites. A stop codon (TGA) has been introduced at L394 to generate the arrestin3-(1-393) truncation mutant by PCR. Arrestin-3 proteins were expressed in BL21 Gold bacterial cells and full-length arrestin-3 was purified as described.<sup>64</sup> Arrestin3-(1-393), which failed to interact with Q-Sepharose, was purified by a modified procedure. Arrestin3-(1-393) was eluted from heparin-Sepharose and loaded onto a Q-Sepharose column while diluting the sample with column buffer (10 mM Tris-HCl, pH 7.5, 2 mM EDTA, 2 mM EGTA, 2 mM benzamidine, 1 mM PMSF, 4 mM DTT) to a final concentration of 10 mM NaCl. The flow-through containing the majority of arrestin-3-(1-393) was loaded directly onto an SP-Sepharose column, which was washed with column buffer (as above

but containing 100 mM NaCl) and then eluted with a 400 ml linear gradient of 100 mM NaCl to 500 mM NaCl. Eluted arrestin-3-(1-393) (peak at ~320 mM NaCl) was concentrated and further purified by gel filtration on a Superdex S200 column equilibrated in 10 mM Tris (pH 7.5), 150 mM NaCl, 2 mM tris(2-carboxyethyl)phosphine (TCEP).

### Crystallization and structure determination of arrestin-3-(1-393)

Arrestin3-(1-393) was concentrated to 12 mg/mL and crystallized from 50 mM Hepes, 675 mM Na/K tartrate, pH 7.5 by the hanging-drop, vapor-diffusion technique. Crystals appeared in 48 h and were harvested after two weeks. The crystals were preserved by stepwise (5% steps) transfer from mother liquor to mother liquor containing 30% (v/v) glycerol and then freezing in liquid nitrogen. Data were collected at the 24-ID-C beamline at the Advanced Photon Source (Argonne, IL) then integrated and scaled with HKL2000.<sup>65</sup> The phases were determined by molecular replacement using PHASER<sup>66</sup> and the 1G4M structure.<sup>21</sup> The search model included amino acid residues 5–357. Water molecules and the C-terminal tail were removed manually, and non-conserved side chains were truncated to C $\beta$  using the program CHAINSAW<sup>67</sup> as implemented in CCP4.<sup>68</sup> The structure was manually rebuilt in COOT<sup>69</sup> using simulated annealing composite omit maps calculated in CNS.<sup>70,71</sup> The structure was refined in Phenix,<sup>72</sup> using non-crystallographic restraints between the two chains, and using 10 TLS groups identified with the TLS motion determination webserver.<sup>73,74</sup> The refinement strategy included positional refinement, simulated annealing, and group B-factor refinement. This strategy, as implemented in Phenix, makes use of maximum likelihood weighting of the errors associated with measured reflections, allowing proper weighting of weak data and hence its inclusion in refinement.<sup>75</sup> Estimates for upper limits of mean positional error were obtained by the Luzzatti method (a plot of *R*-factor versus reciprocal resolution)<sup>76</sup> with improvements allowing for the potential incompleteness of the model (SigmaA)<sup>77</sup> and for different error distributions for different atoms (maximum likelihood).<sup>78</sup> Refinement statistics and error estimates are given in Table 1. The structure was analyzed using PISA,<sup>79</sup> THESEUS<sup>80</sup> and PyMOL<sup>†,81</sup> and the figures were prepared using PyMOL.<sup>81</sup>

### Plasmid construction for bioluminescence energy transfer (BRET)

Plasmid g3NVE-1 containing the sequence of arrestin-3 N-terminally tagged with Venus (a variant of enhanced yellow fluorescent protein,<sup>33</sup> a generous gift from Dr J. A. Javitch, Columbia University), was constructed using a modified pGEM2 *in vitro* transcription vector (Promega; Madison, WI) that contains, under control of the SP6 promoter, an "idealized" 5'-untranslated region<sup>82</sup> with an upstream EcoRI site followed by the coding sequence of bovine arrestin-3 between NcoI and HindIII sites. Venus was amplified by PCR using the forward primer that adds

† [www.pymol.org](http://www.pymol.org)



EcoRI and AsiSI sites upstream of the start codon and the reverse primer that codes for a short spacer with the SGLKSRRALDS sequence and an in-frame NcoI site:

forward: 5'-AGTCAGAATTCGCGATCGCGGCCAC-GATGGTGAGCAAGGGCGA-3'  
reverse: 5'-TCTCCCCCATGGAGTCGAGCGCTCGCC-GAGACTTAAGTCCGGAGGTGGCCT-3'

Venus was subcloned between EcoRI and NcoI restriction sites. Different arrestins were subcloned in-frame with the Venus spacer sequence using NcoI and HindIII sites. The Venus-arrestin fusion proteins were subcloned into a modified pcDNA3 mammalian expression vector (Invitrogen; Carlsbad, CA) using the EcoRI and HindIII restriction sites to generate the P3VEA2-5 and P3VEA3-1 plasmids encoding arrestin-2 and arrestin-3, respectively. Clones encoding arrestin-2-6M and arrestin-3-6M mutants were made by PCR in pGEM2, sequenced, and subcloned into pcDNA3. A plasmid encoding *Renilla* luciferase variant 8 (RLuc8)<sup>83</sup> was a generous gift from Dr Nevin A. Lambert (Medical College of Georgia). RLuc8 was fused in-frame with the sequence of triple HA-tagged human  $\beta$ 2AR (cDNA resource center§). To this end, the coding sequence of  $\beta$ 2AR was amplified by PCR using the forward primer that introduces EcoRI and AsiSI restriction sites upstream of the receptor start codon and the reverse primer that introduces an in-frame SbfI restriction site, which was subcloned using EcoRI and SbfI sites in-frame with C-terminal RLuc8, yielding the P3HB2ALuc-2 plasmid:

forward: 5'-GCTAGAATTCTGCGATCGCACCAC-CATGGCGTACCCATACGATGTCCA-3'  
reverse: 5'-AGCGGAAGCTTCTAGCCTGCAGGTGC-CAGCAGTGAGTCATTG-3'

### BRET assays

The well established BRET1 assay with Venus as the acceptor and RLuc8 as the donor was used to characterize the binding of arrestins to  $\beta$ 2AR-RLuc8.<sup>35–37,84</sup> COS-7 cells were transfected with the indicated plasmids using Lipofectamine™ 2000 (Invitrogen; Carlsbad, CA), according to the manufacturer's protocol (3  $\mu$ L of Lipofectamine™ 2000/1  $\mu$ g of DNA). Increasing amounts of the indicated Venus-arrestin constructs (0–12  $\mu$ g) along with 250 ng of P3HB2ALuc-2 and empty pcDNA3 to equalize DNA were used to transfect 80%–90% confluent COS-7 cells on 60 mm dishes. At 24 h post transfection, cells were trypsinized and seeded at 100,000–200,000 cells/well into white opaque 96-well microplates (Nunc, Rochester, NY) for luminescence measurements or black opaque microplates (Nunc) for fluorescence determination. At 48 h post transfection, the medium was replaced by PBS with  $\text{Ca}^{2+}$  and  $\text{Mg}^{2+}$  containing 0.01% (w/v) glucose, 36 mg/L sodium pyruvate and 25 mM Hepes, pH 7.2. Coelenterazine-*h* (DiscoveRx, Fremont, CA) was added to a final concentration of 5  $\mu$ M at 8 min after agonist (25  $\mu$ M isoproterenol) stimulation, and luminescence was measured immediately using a POLARstar

Optima dual-channel luminometer and fluorimeter microplate reader (BMG Labtech, Cary, NC). The light emitted by coelenterazine-*h* and Venus in each well was measured simultaneously five times through a 465–485 nm bandpass filter and through a 522.5–547.5 nm bandpass filter, respectively. The net BRET ratio was calculated as the long wavelength emission divided by the short wavelength emission, which was expressed as the relative change compared to unstimulated cells. The expression of each Venus-arrestin was evaluated using fluorescence at 535 nm upon excitation by 485 nm. The Venus-arrestin fluorescence, which is directly proportional to the expression levels, was normalized by the basal luminescence from the  $\beta$ 2AR-RLuc8 to account for variation of cell number and expression levels. The curves resulting from the titration of the various amounts of Venus-arrestin were fit by non-linear regression to a one-site hyperbola model using Prism version 5.04 (GraphPad Software, San Diego, CA). A global fit algorithm was used to assess the difference between the respective wild type and mutant arrestins curves.

### Protein Data Bank accession number

Coordinates and structure factors have been deposited in the Protein Data Bank with accession number 3P2D.

### Acknowledgements

The authors are grateful to Dr Jonathan A. Javitch for expert advice on receptor-arrestin BRET and the plasmid encoding Venus, Dr Nevin A. Lambert for the plasmid encoding *Renilla* luciferase variant 8, and Dr Carl Johnson for use of the POLARstar Optima dual channel luminometer and fluorimeter microplate reader. This study was supported, in part, by NIH grants GM077561, GM081756 (to V.V.G.) and GM081778 (to B.W.S.).

### References

1. Gurevich, E. V. & Gurevich, V. V. (2006). Arrestins: ubiquitous regulators of cellular signaling pathways. *Genome Biol.* **7**, 236.
2. Strissel, K. J., Sokolov, M., Trieu, L. H. & Arshavsky, V. Y. (2006). Arrestin translocation is induced at a critical threshold of visual signaling and is superstoichiometric to bleached rhodopsin. *J. Neurosci.* **26**, 1146–1153.
3. Hanson, S. M., Gurevich, E. V., Vishnivetskiy, S. A., Ahmed, M. R., Song, X. & Gurevich, V. V. (2007). Each rhodopsin molecule binds its own arrestin. *Proc. Natl Acad. Sci. USA*, **104**, 3125–3128.
4. Nikonov, S. S., Brown, B. M., Davis, J. A., Zuniga, F. I., Bragin, A., Pugh, E. N., Jr & Craft, C. M. (2008). Mouse cones require an arrestin for normal inactivation of phototransduction. *Neuron*, **59**, 462–474.

5. Gurevich, V. V. & Gurevich, E. V. (2006). The structural basis of arrestin-mediated regulation of G-protein-coupled receptors. *Pharmacol. Ther.* **110**, 465–502.
6. Gurevich, E. V., Benovic, J. L. & Gurevich, V. V. (2002). Arrestin2 and arrestin3 are differentially expressed in the rat brain during postnatal development. *Neuroscience*, **109**, 421–436.
7. Gurevich, E. V., Benovic, J. L. & Gurevich, V. V. (2004). Arrestin2 expression selectively increases during neural differentiation. *J. Neurochem.* **91**, 1404–1416.
8. Goodman, O. B., Jr, Krupnick, J. G., Santini, F., Gurevich, V. V., Penn, R. B., Gagnon, A. W. *et al.* (1996).  $\beta$ -Arrestin acts as a clathrin adaptor in endocytosis of the  $\beta_2$ -adrenergic receptor. *Nature*, **383**, 447–450.
9. Laporte, S. A., Oakley, R. H., Zhang, J., Holt, J. A., Ferguson, S. S. G., Caron, M. G. & Barak, L. S. (1999). The 2-adrenergic receptor/arrestin complex recruits the clathrin adaptor AP-2 during endocytosis. *Proc. Natl Acad. Sci. USA*, **96**, 3712–3717.
10. DeWire, S. M., Ahn, S., Lefkowitz, R. J. & Shenoy, S. K. (2007).  $\beta$ -Arrestins and cell signaling. *Annu. Rev. Physiol.* **69**, 483–510.
11. Gurevich, V. V., Richardson, R. M., Kim, C. M., Hosey, M. M. & Benovic, J. L. (1993). Binding of wild type and chimeric arrestins to the m2 muscarinic cholinergic receptor. *J. Biol. Chem.* **268**, 16879–16882.
12. Gurevich, V. V. (1998). The selectivity of visual arrestin for light-activated phosphorhodopsin is controlled by multiple nonredundant mechanisms. *J. Biol. Chem.* **273**, 15501–15506.
13. Gurevich, V. V., Dion, S. B., Onorato, J. J., Ptasienski, J., Kim, C. M., Sterne-Marr, R. *et al.* (1995). Arrestin interaction with G protein-coupled receptors. Direct binding studies of wild type and mutant arrestins with rhodopsin, b2-adrenergic, and m2 muscarinic cholinergic receptors. *J. Biol. Chem.* **270**, 720–731.
14. Celver, J., Vishnivetskiy, S. A., Chavkin, C. & Gurevich, V. V. (2002). Conservation of the phosphate-sensitive elements in the arrestin family of proteins. *J. Biol. Chem.* **277**, 9043–9048.
15. Kovoov, A., Celver, J., Abdryashitov, R. I., Chavkin, C. & Gurevich, V. V. (1999). Targeted construction of phosphorylation-independent  $\beta$ -arrestin mutants with constitutive activity in cells. *J. Biol. Chem.* **274**, 6831–6834.
16. Pan, L., Gurevich, E. V. & Gurevich, V. V. (2003). The nature of the arrestin x receptor complex determines the ultimate fate of the internalized receptor. *J. Biol. Chem.* **278**, 11623–11632.
17. Kohout, T. A., Lin, F. S., Perry, S. J., Conner, D. A. & Lefkowitz, R. J. (2001).  $\beta$ -Arrestin 1 and 2 differentially regulate heptahelical receptor signaling and trafficking. *Proc. Natl Acad. Sci. USA*, **98**, 1601–1606.
18. Oakley, R. H., Laporte, S. A., Holt, J. A., Caron, M. G. & Barak, L. S. (2000). Differential affinities of visual arrestin, barrestin1, and barrestin2 for G protein-coupled receptors delineate two major classes of receptors. *J. Biol. Chem.* **275**, 17201–17210.
19. Granzin, J., Wilden, U., Choe, H. W., Labahn, J., Krafft, B. & Buldt, G. (1998). X-ray crystal structure of arrestin from bovine rod outer segments. *Nature*, **391**, 918–921.
20. Hirsch, J. A., Schubert, C., Gurevich, V. V. & Sigler, P. B. (1999). The 2.8 Å crystal structure of visual arrestin: a model for arrestin's regulation. *Cell*, **97**, 257–269.
21. Han, M., Gurevich, V. V., Vishnivetskiy, S. A., Sigler, P. B. & Schubert, C. (2001). Crystal structure of  $\beta$ -arrestin at 1.9 Å: possible mechanism of receptor binding and membrane translocation. *Structure*, **9**, 869–880.
22. Kang, D. S., Kern, R. C., Puthenveedu, M. A., von Zastrow, M., Williams, J. C. & Benovic, J. L. (2009). Structure of an arrestin2-clathrin complex reveals a novel clathrin binding domain that modulates receptor trafficking. *J. Biol. Chem.* **284**, 29860–29872.
23. Milano, S. K., Kim, Y. M., Stefano, F. P., Benovic, J. L. & Brenner, C. (2006). Nonvisual arrestin oligomerization and cellular localization are regulated by inositol hexakisphosphate binding. *J. Biol. Chem.* **281**, 9812–9823.
24. Milano, S. K., Pace, H. C., Kim, Y. M., Brenner, C. & Benovic, J. L. (2002). Scaffolding functions of arrestin-2 revealed by crystal structure and mutagenesis. *Biochemistry*, **41**, 3321–3328.
25. Sutton, R. B., Vishnivetskiy, S. A., Robert, J., Hanson, S. M., Raman, D., Knox, B. E. *et al.* (2005). Crystal structure of cone arrestin at 2.3 Å: evolution of receptor specificity. *J. Mol. Biol.* **354**, 1069–1080.
26. Vishnivetskiy, S. A., Hosey, M. M., Benovic, J. L. & Gurevich, V. V. (2004). Mapping the arrestin-receptor interface: structural elements responsible for receptor specificity of arrestin proteins. *J. Biol. Chem.* **279**, 1262–1268.
27. Vishnivetskiy, S. A., Hirsch, J. A., Velez, M. G., Gurevich, Y. V. & Gurevich, V. V. (2002). Transition of arrestin in the active receptor-binding state requires an extended interdomain hinge. *J. Biol. Chem.* **277**, 43961–43968.
28. Vishnivetskiy, S. A., Paz, C. L., Schubert, C., Hirsch, J. A., Sigler, P. B. & Gurevich, V. V. (1999). How does arrestin respond to the phosphorylated state of rhodopsin. *J. Biol. Chem.* **274**, 11451–11454.
29. Pulvermuller, A., Schroder, K., Fischer, T. & Hofmann, K. P. (2000). Interactions of metarhodopsin II. Arrestin peptides compete with arrestin and transducin. *J. Biol. Chem.* **275**, 37679–37685.
30. Hanson, S. M., Francis, D. J., Vishnivetskiy, S. A., Klug, C. S. & Gurevich, V. V. (2006). Visual arrestin binding to microtubules involves a distinct conformational change. *J. Biol. Chem.* **281**, 9765–9772.
31. Hanson, S. M. & Gurevich, V. V. (2006). The differential engagement of arrestin surface charges by the various functional forms of the receptor. *J. Biol. Chem.* **281**, 3458–3462.
32. Miller, W. E., McDonald, P. H., Cai, S. F., Field, M. E., Davis, R. J. & Lefkowitz, R. J. (2001). Identification of a motif in the carboxyl terminus of  $\beta$ -arrestin2 responsible for activation of JNK3. *J. Biol. Chem.* **276**, 27770–27777.
33. Nagai, T., Ibata, K., Park, E. S., Kubota, M., Mikoshiba, K. & Miyawaki, A. (2002). A variant of yellow fluorescent protein with fast and efficient maturation for cell-biological applications. *Nat. Biotechnol.* **20**, 87–90.
34. Barak, L. S., Ferguson, S. S., Zhang, J. & Caron, M. G. (1997). A  $\beta$ -arrestin/green fluorescent protein biosen-

- sensor for detecting G protein-coupled receptor activation. *J. Biol. Chem.* **272**, 27497–27500.
35. Kuravi, S., Lan, T. H., Barik, A. & Lambert, N. A. (2010). Third-party bioluminescence resonance energy transfer indicates constitutive association of membrane proteins: application to class a g-protein-coupled receptors and g-proteins. *Biophys. J.* **98**, 2391–2399.
36. Namkung, Y., Dipace, C., Urizar, E., Javitch, J. A. & Sibley, D. R. (2009). G protein-coupled receptor kinase-2 constitutively regulates D2 dopamine receptor expression and signaling independently of receptor phosphorylation. *J. Biol. Chem.* **284**, 34103–34115.
37. Namkung, Y., Dipace, C., Javitch, J. A. & Sibley, D. R. (2009). G protein-coupled receptor kinase-mediated phosphorylation regulates post-endocytic trafficking of the D2 dopamine receptor. *J. Biol. Chem.* **284**, 15038–15051.
38. Schubert, C., Hirsch, J. A., Gurevich, V. V., Engelman, D. M., Sigler, P. B. & Fleming, K. G. (1999). Visual arrestin activity may be regulated by self-association. *J. Biol. Chem.* **274**, 21186–21190.
39. Imamoto, Y., Tamura, C., Kamikubo, H. & Kataoka, M. (2003). Concentration-dependent tetramerization of bovine visual arrestin. *Biophys. J.* **85**, 1186–1195.
40. Hanson, S. M., Vishnivetskiy, S. A., Hubbell, W. L. & Gurevich, V. V. (2008). Opposing effects of inositol hexakisphosphate on rod arrestin and arrestin2 self-association. *Biochemistry*, **47**, 1070–1075.
41. Ponstingl, H., Henrick, K. & Thornton, J. M. (2000). Discriminating between homodimeric and monomeric proteins in the crystalline state. *Proteins: Struct. Funct. Genet.* **41**, 47–57.
42. Shi, H., Rojas, R., Bonifacino, J. S. & Hurley, J. H. (2006). The retromer subunit Vps26 has an arrestin fold and binds Vps35 through its C-terminal domain. *Nat. Struct. Mol. Biol.* **13**, 540–548.
43. Collins, B. M., Norwood, S. J., Kerr, M. C., Mahony, D., Seaman, M. N., Teasdale, R. D. & Owen, D. J. (2008). Structure of Vps26B and mapping of its interaction with the retromer protein complex. *Traffic*, **9**, 366–379.
44. Attramadal, H., Arriza, J. L., Aoki, C., Dawson, T. M., Codina, J., Kwatra, M. M. *et al.* (1992).  $\beta$ -Arrestin2, a novel member of the arrestin/ $\beta$ -arrestin gene family. *J. Biol. Chem.* **267**, 17882–17890.
45. Sterne-Marr, R., Gurevich, V. V., Goldsmith, P., Bodine, R. C., Sanders, C., Donoso, L. A. & Benovic, J. L. (1993). Polypeptide variants of  $\beta$ -arrestin and arrestin3. *J. Biol. Chem.* **268**, 15640–15648.
46. Barnes, W. G., Reiter, E., Violin, J. D., Ren, X. R., Milligan, G. & Lefkowitz, R. J. (2005).  $\beta$ -Arrestin 1 and G $\alpha_q$ /11 coordinately activate RhoA and stress fiber formation following receptor stimulation. *J. Biol. Chem.* **280**, 8041–8050.
47. Povsic, T. J., Kohout, T. A. & Lefkowitz, R. J. (2003).  $\beta$ -Arrestin1 mediates insulin-like growth factor 1 (IGF-1) activation of phosphatidylinositol 3-kinase (PI3K) and anti-apoptosis. *J. Biol. Chem.* **278**, 51334–51339.
48. Nobles, K. N., Guan, Z., Xiao, K., Oas, T. G. & Lefkowitz, R. J. (2007). The active conformation of  $\beta$ -arrestin1: direct evidence for the phosphate sensor in the N-domain and conformational differences in the active states of  $\beta$ -arrestins1 and -2. *J. Biol. Chem.* **282**, 21370–21381.
49. Schumann, M., Nakagawa, T., Mantey, S. A., Howell, B. & Jensen, R. T. (2008). Function of non-visual arrestins in signaling and endocytosis of the gastrin-releasing peptide receptor (GRP receptor). *Biochem. Pharmacol.* **75**, 1170–1185.
50. Gurevich, V. V. & Gurevich, E. V. (2004). The molecular acrobatics of arrestin activation. *Trends Pharmacol. Sci.* **25**, 59–112.
51. Vishnivetskiy, S. A., Schubert, C., Climaco, G. C., Gurevich, Y. V., Velez, M. G. & Gurevich, V. V. (2000). An additional phosphate-binding element in arrestin molecule: implications for the mechanism of arrestin activation. *J. Biol. Chem.* **275**, 41049–41057.
52. Song, X., Coffa, S., Fu, H. & Gurevich, V. V. (2009). How does arrestin assemble MAP kinases into a signaling complex. *J. Biol. Chem.* **284**, 685–695.
53. Song, X., Gurevich, E. V. & Gurevich, V. V. (2007). Cone arrestin binding to JNK3 and Mdm2: conformational preference and localization of interaction sites. *J. Neurochem.* **103**, 1053–1062.
54. Song, X., Raman, D., Gurevich, E. V., Vishnivetskiy, S. A. & Gurevich, V. V. (2006). Visual and both non-visual arrestins in their “inactive” conformation bind JNK3 and Mdm2 and relocate them from the nucleus to the cytoplasm. *J. Biol. Chem.* **281**, 21491–21499.
55. McDonald, P. H., Chow, C. W., Miller, W. E., Laporte, S. A., Field, M. E., Lin, F. T. *et al.* (2000).  $\beta$ -Arrestin 2: a receptor-regulated MAPK scaffold for the activation of JNK3. *Science*, **290**, 1515–1518.
56. Gurevich, V. V. & Gurevich, E. V. (2010). Custom-designed proteins as novel therapeutic tools? The case of arrestins. *Expert Rev. Mol. Med.* **12**, e13.
57. Donoso, L. A., Gregerson, D. S., Smith, L., Robertson, S., Knospe, V., Vrabec, T. & Kalsow, C. M. (1990). S-Sntigen: preparation and characterization of site-specific monoclonal antibodies. *Curr. Eye Res.* **9**, 343–355.
58. Hanson, S. M., Van Eps, N., Francis, D. J., Altenbach, C., Vishnivetskiy, S. A., Arshavsky, V. Y. *et al.* (2007). Structure and function of the visual arrestin oligomer. *EMBO J.* **26**, 1726–1736.
59. Hanson, S. M., Dawson, E. S., Francis, D. J., Van Eps, N., Klug, C. S., Hubbell, W. L. *et al.* (2008). A model for the solution structure of the rod arrestin tetramer. *Structure*, **16**, 924–934.
60. Nair, K. S., Hanson, S. M., Kennedy, M. J., Hurley, J. B., Gurevich, V. V. & Slepak, V. Z. (2004). Direct binding of visual arrestin to microtubules determines the differential subcellular localization of its splice variants in rod photoreceptors. *J. Biol. Chem.* **279**, 41240–41248.
61. Nair, K. S., Hanson, S. M., Mendez, A., Gurevich, E. V., Kennedy, M. J., Shestopalov, V. I. *et al.* (2005). Light-dependent redistribution of arrestin in vertebrate rods is an energy-independent process governed by protein-protein interactions. *Neuron*, **46**, 555–567.
62. Storez, H., Scott, M. G., Issafras, H., Burtey, A., Benmerah, A., Muntaner, O. *et al.* (2005). Homo- and hetero-oligomerization of  $\beta$ -arrestins in living cells. *J. Biol. Chem.* **280**, 40210–40215.
63. DeFea, K. A. (2008).  $\beta$ -Arrestin multimers: does a crowd help or hinder function? *Biochem. J.* **413**, e1–e3.
64. Gurevich, V. V. & Benovic, J. L. (2000). Arrestin: mutagenesis, expression, purification, and functional characterization. *Methods Enzymol.* **315**, 422–437.



65. Otwinowski, Z. & Minor, W. (1997). Processing of X-ray diffraction data collected in oscillation mode. *Methods Enzymol.* **276**, 307–326.
66. McCoy, A. J., Grosse-Kunstleve, R. W., Storoni, L. C. & Read, R. J. (2005). Likelihood-enhanced fast translation functions. *Acta Crystallogr. D*, **61**, 458–464.
67. Stein, N. (2008). CHAINSAW: a program for mutating pdb files used as templates in molecular replacement. *J. Appl. Crystallogr.* **41**, 641–643.
68. Collaborative Computational Project Number 4. (1994). The CCP4 suite - programs for protein crystallography. *Acta Crystallogr. D*, **50**, 760–763.
69. Emsley, P. & Cowtan, K. (2004). Coot: model-building tools for molecular graphics. *Acta Crystallogr. D*, **60**, 2126–2132.
70. Brünger, A. T., Adams, P. D. & Rice, L. M. (1997). New applications of simulated annealing in X-ray crystallography and solution NMR. *Structure*, **5**, 325–336.
71. Brünger, A. T., Adams, P. D., Clore, G. M., DeLano, W. L., Gros, P., Grosse-Kunstleve, R. W. *et al.* (1998). Crystallography & NMR system: a new software suite for macromolecular structure determination. *Acta Crystallogr. D*, **54**, 905–921.
72. Adams, P. D., Grosse-Kunstleve, R. W., Hung, L. W., Ioerger, T. R., McCoy, A. J., Moriarty, N. W. *et al.* (2002). PHENIX: building new software for automated crystallographic structure determination. *Acta Crystallogr. D*, **58**, 1948–1954.
73. Painter, J. & Merritt, E. A. (2006). Optimal description of a protein structure in terms of multiple groups undergoing TLS motion. *Acta Crystallogr. D*, **62**, 439–450.
74. Painter, J. & Merritt, E. A. (2006). TLSMD web server for the generation of multi-group TLS models. *J. Appl. Crystallogr.* **39**, 109–111.
75. Pannu, N. S. & Read, R. J. (1996). Improved structure refinement through maximum likelihood. *Acta Crystallogr. A*, **52**, 659–668.
76. Luzzati, V. P. (1953). Resolution d'une structure cristalline lorsque les positions d'une partie des atomes sont connues: traitement statistique. *Acta Crystallogr.* **6**, 731–736.
77. Read, R. J. (1986). Improved Fourier coefficients for maps using phases from partial structures with errors. *Acta Crystallogr. A*, **42**, 140–144.
78. Adams, P. D., Afonine, P. V., Grosse-Kunstleve, R. W., Read, R. J., Richardson, J. S., Richardson, D. C. & Terwilliger, T. C. (2009). Recent developments in phasing and structure refinement for macromolecular crystallography. *Curr. Opin. Struct. Biol.* **19**, 566–572.
79. Krissinel, E. & Henrick, K. (2007). Inference of macromolecular assemblies from crystalline state. *J. Mol. Biol.* **372**, 774–797.
80. Theobald, D. L. & Wuttke, D. S. (2006). THESEUS: maximum likelihood superpositioning and analysis of macromolecular structures. *Bioinformatics*, **22**, 2171–2172.
81. DeLano, W. L. (2002). *The PyMOL Molecular Graphics System*. DeLano Scientific, San Carlos, CA.
82. Gurevich, V. V. (1996). Use of bacteriophage RNA polymerase in RNA synthesis. *Methods Enzymol.* **275**, 382–397.
83. Loening, A. M., Fenn, T. D., Wu, A. M. & Gambhir, S. S. (2006). Consensus guided mutagenesis of Renilla luciferase yields enhanced stability and light output. *Protein Eng. Des. Sel.* **19**, 391–400.
84. Kocan, M. & Pfeleger, K. D. (2009). Detection of GPCR/ $\beta$ -arrestin interactions in live cells using bioluminescence resonance energy transfer technology. *Methods Mol. Biol.* **552**, 305–317.